LOCALLY WEIGHTED TOTAL VARIATION DENOISING FOR PSF MODELING ARTIFACT SUPPRESSION IN PET RECONSTRUCTION

Arthur Mikhno[1], *Elsa D. Angelini*[1,2], *and Andrew F. Laine*[1]

1. Department of Biomedical Engineering, Columbia University, New York
2. Institut Mines-Telecom, Telecom ParisTech, CNRS LTCI, Paris, France

ABSTRACT

Incorporating the point spread function (PSF) into the iterative MLEM reconstruction of PET images introduces contrast and size dependent ringing and over enhancement artifacts. We previously developed a new method, called TV-PSF-MLEM, to suppress these artifacts based on the introduction of a locally-weighted total variation regularization within the MLEM reconstruction algorithm. On non-noisy PET measures, we proposed to compute the TV spatial weights based on the point-wise convergence rate of a preliminary MLEM reconstruction, for each voxel. In this work we extend the TV-PSF-MLEM weighting scheme to noisy measures introducing a noise-independent weighting scheme. We compare its performance to a state of the art PET denoising method. Results on numerical phantoms show that the TV-PSF-MLEM offers substantial advantages in the recovery of small cylinders and gains in contrast recovery of larger cylinders.

Index Terms— PET, image reconstruction, point spread function, MLEM, Total Variation

1. INTRODUCTION

Iterative reconstruction techniques, such as the maximum likelihood expectation maximization (MLEM), provide a flexible framework in positron emission tomography (PET) imaging for modeling the physics and the scanner geometry, yielding greater image contrast, visual quality and noise robustness than analytical reconstruction methods. Incorporating the point spread function (PSF) of the scanner into the iterative MLEM reconstruction process (called PSF-MLEM) improves spatial resolution but introduces significant contrast and size dependent over-enhancement and ringing artifacts [1, 2]. The over-enhancement artifacts might be explained by the mismatch between the true and the measured PSF, while the ringing artifacts are related to object sizes [3]. Most approaches previously proposed to compensate ringing artifacts tend to blur the PET data which undermines the benefits of including the PSF in the reconstruction [3].

A promising approach was recently proposed by Rapisarda *et al.* for artifact suppression by incorporating a new regularization prior into the reconstruction process that locally modifies the image estimate at each iteration in an attempt to locally control edge enhancement [4]. This method provides excellent ringing suppression in the image, especially for large structures, but also tends to suppress the benefits of PSF modeling in smaller objects.

We previously developed a new method (called TV-PSF-MLEM) to suppress PSF-MLEM artifacts based on a locally weighted total variation regularization applied at each iteration [5]. Amplitude of the weights specify the amount of TV regularization at each voxel. These local weights can be precalculated based on the convergence rate of MLEM at each voxel since we established that the convergence rate is directly related to the object size and contrast and that artifact magnitudes are directly proportional to this convergence rate. Using noiseless simulations, we showed that TV-PSF-MLEM suppress ringing artifact while providing edge and contrast recovery, beyond that of standard MLEM, especially in small cylinders. In this paper we extend the TV-PSF-MLEM formalism to simulations corrupted with Poisson noise. A new weighting scheme is introduced robust to noise and results are presented, comparing to the Rapisarda method that is also based on a regularization prior.

2. METHODOLOGY

2.1. Iterative image reconstruction: MLEM algorithm

The ML estimate of the PET image is computed using the MLEM algorithm, and following the notation from [4], leads to the following iterative update equation:

$$\lambda_b^{k+1} = \frac{\lambda_b^k}{BP_b\mathbf{1}} BP_b \frac{y_d}{P_d\lambda_{b'}^k} = \lambda_b^k u_b^k \qquad (1)$$

where λ_b^k represents the intensity of the voxel b within the image λ at iteration k, y_d is the sinogram measure, equal to the number of counts along the line of response (LOR) d, and $\mathbf{1}$ is a unit matrix of the same size as y_d. Following the methodology introduced in [4], incorporating the PSF model into Eq. (1) is achieved by modifying the projector P and backprojector BP as follows:

$$\begin{aligned} P_d(\cdot)_b &= \sum((\cdot) * PSF)_b p_{bd} \\ BP_b(\cdot)_d &= PSF^T \sum(\cdot)_d p_{bd} \end{aligned} \qquad (2)$$

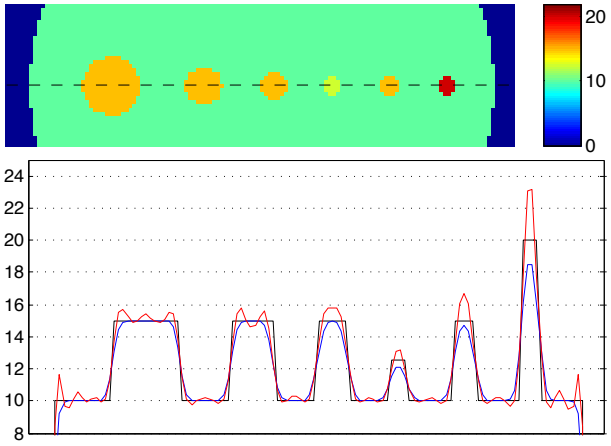

Fig. 1: (top) Middle portion of the simulated cylindrical phantom object with inset cylinders of various diameters. (bottom) Center profiles (along the dashed line above) of reconstructions with MLEM (blue line), PSF-MLEM (red line), and ideal phantom (black line).

where PSF represents the PSF kernel and $*$ is a discretized convolution operator as defined in Appendix of [6]. For a symmetric kernel, $PSF = PSF^T$. Hereafter PSF-MLEM shall refer to the situation when PSF is a non-zero matrix, and MLEM when $PSF = \mathbf{1}$.

2.2. Simulation framework: software and phantom

All methodological developments were performed using simulated sinograms. PET image reconstructions were performed using the STIR open source C++ software (v2.2) [6]. The modified projectors in Eq. (2) were implemented in C++ within the STIR source code. A $200mm$ diameter cylindrical phantom object was simulated, with a background intensity equal to 10, and containing three hot spots of diameter $25mm$, $16mm$, $12mm$ with a 1.5:1 contrast ratio (CR), as well as three $8mm$ diameter hot spots with CR of 1.25:1, 1.5:1 and 2:1, respectively. The phantom was blurred with a symmetrical $4.5mm$ FWHM Gaussian kernel [5] to simulate the resolution loss inherent to the ECAT HR+ scanner (Siemens/CTI) at use in our facility. Figure 1 illustrates the phantom image with resolution and contrast loss due to blurring, as well as the ringing and over-enhancement artifacts of PSF-MLEM. Poisson noise was added to the sinogram measures y_d using the STIR $poisson\_noise$ command with scaling_factor = 1.

2.3. TV regularization prior (Rapisarda method)

A Bayesian formulation of the iterative reconstruction algorithm can be used, leading to a maximum a posteriori (MAP) estimate that includes an *a priori* probability term. Rapisarda proposed the following iterative MAP estimate [4]:

$$\lambda_b^{k+1} = \frac{\lambda_b^k}{BP_b[1 - \alpha D_b \lambda_b^k]} BP_b \frac{y_d}{P_d \lambda_{b'}^k} \tag{3}$$

where $\alpha > 0$ weights the contribution of the value D_b at pixel b of a regularization prior D defined as:

$$D[\lambda] = \nabla \cdot \left(\phi'(|\nabla \lambda|) \frac{\nabla \lambda}{|\nabla \lambda|} \right) \tag{4}$$

The term $\phi'(x)$ is called the variational prior and is based on a modification of the generalized p-Gaussian kernel:

$$\phi'(x) = \begin{cases} x^{(p-1)} & x < \delta \\ 1 - \frac{d(d+\delta)}{d+x} & x \geq \delta \end{cases} \tag{5}$$

where $d = (1 - \delta^{p-1})$, with δ being a gradient threshold.

2.4. TV-PSF-MLEM: algorithm

We introduced in [5] a locally-weighted total variation regularization scheme for PSF-MLEM reconstruction. We outline its components briefly here. Using previous notations, at each iteration of Eq. (1) the total variation problem amounts to finding an estimate image $\hat{\lambda}^k$ that satisfies:

$$\hat{\lambda}^k = \min_{\theta} \frac{1}{2} \left\| \lambda^k - \theta \right\|^2 + \beta \left| \nabla \theta \right| \tag{6}$$

where $|| \cdot ||$ and $| \cdot |$ are the l_2 and l_1 norms, respectively, and β is a positive scalar regularization weight. The classical framework given by Eq. (6) minimizes TV over the whole image. Instead, local weights w_b were introduced for each individual pixels b as follows:
We define $\dot{\lambda}_b^k$ as the locally weighted TV estimate:

$$\dot{\lambda}_b^k = \lambda_b^k + w_b \Delta \hat{\lambda}_b^k \tag{7}$$

where w_b is a spatially-varying weight imposed on the net change of each voxel and $\Delta \hat{\lambda}_b^k$ is defined as:

$$\hat{\lambda}_b^k = \lambda_b^k + (\hat{\lambda}_b^k - \lambda_b^k) = \lambda_b^k + \Delta \hat{\lambda}_b^k \tag{8}$$

Note that if w_b = 1 then $\dot{\lambda}_b = \hat{\lambda}_b$, corresponding to the classical solution to Eq. (6).

We proposed to use the convergence rate, derived from the value of u_b in Eq. (1), for the definition of the spatial weights w_b, as detailed in [5], using the following values:

$$c_b = \min_k |1 - u_b^k| \leq \epsilon$$
$$w_b = 1 - \frac{c_b - \min(c)}{\max(c - \min(c))} \tag{9}$$

where c_b is defined as the earliest MLEM iteration k at which voxel b converges (in practice when $u_b^k \approx 1$), w_b is derived by normalizing c_b such that $0 \leq w_b \leq 1$, and ϵ is a convergence threshold ($\epsilon = 1 \times 10^{-4}$ in [5]). Figure 2 illustrates the spatial TV-weights w_b obtained with this approach for noiseless and noisy measures. PSF-MLEM with TV denoising method (TV-PSF-MLEM) is summarized in Algorithm 1.

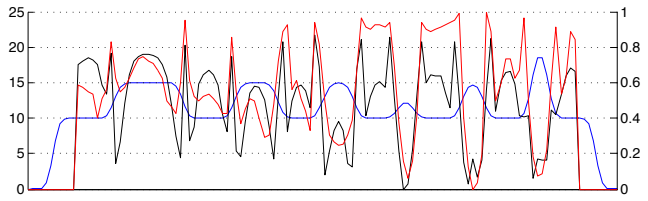

Fig. 2: Local TV weights calculated using Eq. (9) with noiseless data (black line) and using Eq. (10) with noisy data (red line). The profile of the noiseless MLEM reconstruction (blue line) is shown as a reference. Left and right y-axes correspond to MLEM pixel intensities and weights w_b, respectively.

Algorithm 1 TV-PSF-MLEM algorithm

Data: N, λ_0, $k = 0$, **Result**: λ_b^N, **Initialize**: $\lambda_b^0 = \lambda_0$
while $k \leq N$ **do**
$\lambda_b^{k+1} \leftarrow \lambda_b^k$ from Eq. (1)
$\hat{\lambda}_b^{k+1} \leftarrow \lambda_b^{k+1}$ from Eq. (6)
$\dot{\lambda}_b^{k+1} \leftarrow \hat{\lambda}_b^{k+1}$ from Eq. (7)
$\lambda_b^{k+1} \leftarrow \dot{\lambda}_b^{k+1}$, $k \leftarrow k+1$

2.5. TV-PSF-MLEM: TV spatial weights for noisy data

From Eq. (9) it can be seen that weights depend on the convergence rate of individual voxels b and will therefore be highly affected by the presence of noise. To adapt our approach to noisy data, we first studied the oracle approach where ideal weights (derived from the noiseless case) were applied to TV-PSF-MLEM reconstruction of the noisy sinograms, corrupted with Poisson noise. Results, illustrated in Figure 2, show that reconstructions after N=500 iterations were similar with and without noise, with good suppression of noise and ringing artifact, but with some over enhancement of the *8mm* cylinders in both cases. To approximate these oracle weights using the iterative MLEM reconstructions from the noisy data, we propose to use a local spatial aggregation of the convergence rates estimates u_b^k from Eq. (1), using the average kernel of size $n \times n$ with $n = 3$, along with a modified value for ϵ: $\epsilon = 5 \times 10^{-4}$. Results illustrated in Figure 2, show that such approach leads to a profile of the local weights that mimics well the general shape of the oracle weights although local differences in magnitude exist. Thus, the calculation of the parameter c_b used in Eq. (9), on noisy data becomes:

$$\hat{u}_b^k = \sum_{b \in N_b} u_b^k \tag{10}$$

where N_b is the 3x3 neighborhood around voxel b, and $\hat{u}_b^k$ replaces u_b^k in Eq. (9) for noisy data.

3. RESULTS

3.1. Experimental setup using synthetic phantom data

Performance of MLEM, PSF-MLEM, TV-PSF-MLEM, and the Rapisarda method was quantitatively assessed using the

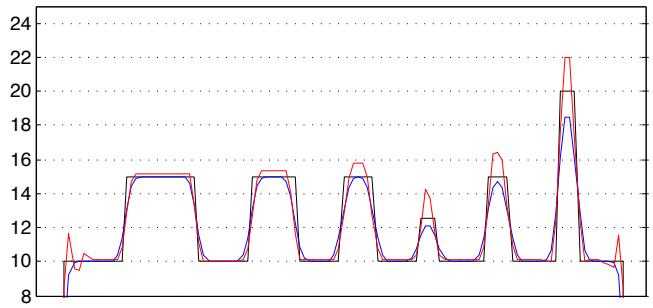

(a) without noise

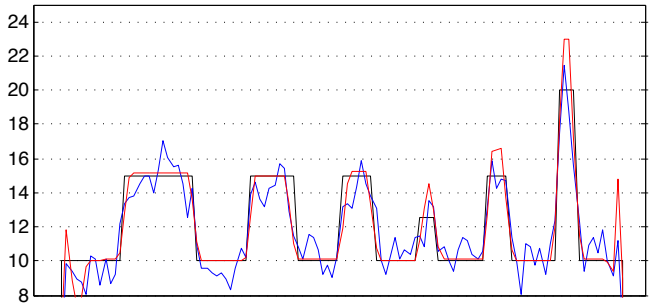

(b) with Poisson noise

Fig. 3: TV-PSF-MLEM reconstruction with oracle weights for simulated phantom without (a) and with (b) added Poisson noise to the sinogram. Horizontal profile lines through the center of the image are shown for ideal phantom (black line), 200 iterations of MLEM using Eq. (1) (blue line), and 500 iterations of TV-PSF-MLEM with oracle weights (red line) initialized with 200 iterations of MLEM.

recovery coefficient defined in Eq. (11). For TV-PSF–MLEM the regularization weight $\beta = 0.02$ was used as in [5], and for the Rapisarda method parameters were set as recommended by the authors in [4]: $p = 1.33$, $\delta = 0.3$, and $\alpha = 0.002$. In an attempt to suppress over-enhancement in the $8mm$ cylinders, as observed in Figure 3, we set a minimum cutoff value for the w_b values (stemming from the observation that w_b in those cylinders were lower than anywhere else in the image). By increasing w_b values we enforce more TV regularization to prevent overshooting. Experiments were run until convergence, corresponding to: N=200 for MLEM and N=500 for TV-PSF-MLEM and Rapisarda.

$$RC = \sum_{b \in \Omega_{ROI}} \lambda_b^{recon} \Big/ \sum_{b \in \Omega_{ROI}} \lambda_b^{true} \tag{11}$$

3.2. Evaluation of artifact suppression

Visually TV-PSF-MLEM and Rapisarda reconstructions provide very comparable results in large cylinders ($\geq 12mm$), as seen in Figure 4. In smaller cylinders, the Rapisarda method underestimates while the TV-PSF-MLEM overestimates the activity. TV-PSF-MLEM appears more homogenous in the background and in larger cylinders. At the outer edges of the

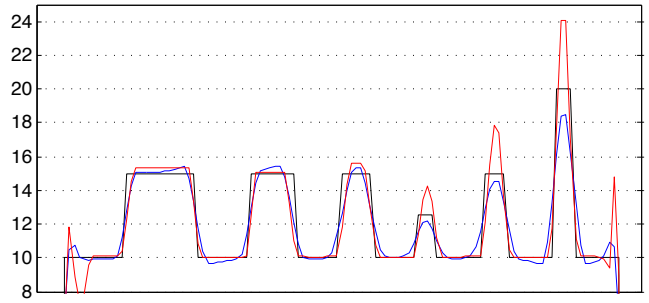

Fig. 4: Reconstruction results on simulated phantom with Poisson noise. Center profile is shown for: (black line) ideal phantom, (blue line) 500 iterations of Rapisarda using Eq. (3) , and (red line) 500 iterations of TV-PSF-MLEM with average weights calculated using Eq. (10). Reconstructions were initialized with 200 MLEM iterations.

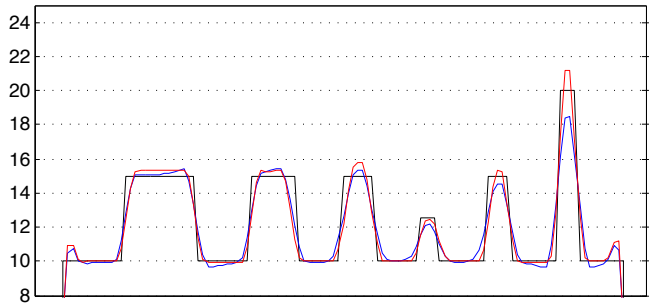

Fig. 5: Reconstruction results on simulated phantom with Poisson noise and w_b cutoff value. Center profile is shown for: (black line) ideal phantom, (blue line) 500 iterations of Rapisarda Eq. (3), and (red line) 500 iterations of TV-PSF-MLEM with average weights, Eq. (10), and w_b cutoff=0.2. Reconstructions were initialized with 200 MLEM iterations.

phantoms artifacts in the TV-PSF-MLEM reconstruction are due to the non regularization with local weights w_b there. The overshoot in small cylinders and background edges is largely remedied by applying a simple cutoff, as shown in Figure 5.

The performance characteristic of the two methods is better understood in terms of RC values, reported in Figure 6 for the different cylinders. The Rapisarda method yields RCs for all cylinders that closely track the noiseless MLEM estimate, with slightly higher RCs for cylinder diameters $\geq 12mm$, and outperforming standard MLEM on noisy data. Hence this method provides excellent noise suppression but greatly limits the contrast enhancement gained from PSF modeling as it does not recover contrast loss due to blurring effects. In contrast, TV-PSF-MLEM (with or without cutoff on the w_b) yields higher RC values for all cylinders. For the $24mm$ and $8mm$ cylinders the recovery level on noisy data approaches the recovery level of PSF-MLEM without noise. When a cutoff value is applied on the w_b, all RC values are higher than with the Rapisarda method, especially in the highest contrast $8mm$ cylinder.

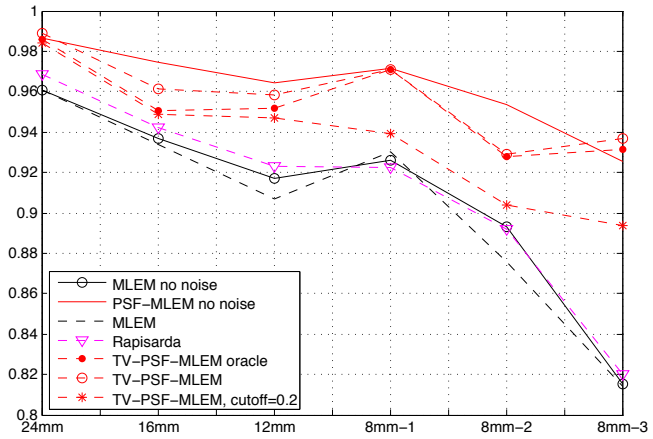

Fig. 6: Recovery Coefficients (RC) of cylinders (x-axis) with different reconstruction methods on noisy (dashed lines) and non-noisy (solid lines) data. MLEM and PSF-MLEM are shown on non-noisy data as references for the expected worst and best RC value.

4. CONCLUSIONS

We compared two ML iterative PET reconstruction algorithms that both exploit local regularization of the image data: our proposed TV-PSF-MLEM method and the Rapisarda method described in [4]. Our simulation results demonstrate that in the presence of noise, our proposed method is robust and provides advantages in terms of visual quality and contrast recovery, especially in small structures. Further testing with varying levels of noise, higher contrast ratios, real phantom objects and clinical data is planned.

5. REFERENCES

[1] B. Bai and P. D. Esser, "The effect of edge artifacts on quantification of positron emission tomography," in *Nuclear Science Symposium Conference Record (NSS/MIC), 2010 IEEE*, 2010, p. 22632266.

[2] K. Thielemans, E. Asma, S. Ahn, R. M. Manjeshwar, T. Deller, S. G. Ross, C. W. Stearns, and A. Ganin, "Impact of PSF modelling on the convergence rate and edge behaviour of EM images in PET," in *Nuclear Science Symposium Conference Record (NSS/MIC), 2010 IEEE*, 2010, p. 32673272.

[3] Shan Tong, Adam M. Alessio, Kris Thielemans, Charles Stearns, Steve Ross, and Paul E. Kinahan, "Properties and mitigation of edge artifacts in PSF-Based PET reconstruction," *IEEE Transactions on Nuclear Science*, vol. 58, no. 5, pp. 2264–2275, Oct. 2011.

[4] Eugenio Rapisarda, Valentino Bettinardi, Kris Thielemans, and Maria Carla Gilardi, "Evaluation of a new regularization prior for 3-d PET reconstruction including PSF modeling," *IEEE Transactions on Nuclear Science*, vol. 59, no. 1, pp. 88–101, Feb. 2012.

[5] Arthur Mikhno, Elsa D Angelini, Bing Bai, and Andrew F Laine, "Locally weighted total variation denoising for ringing artifact suppression in pet reconstruction using psf modeling," in *Biomedical Imaging (ISBI), 2013 IEEE 10th International Symposium on*. IEEE, 2013, pp. 1252–1255.

[6] Kris Thielemans, Charalampos Tsoumpas, Sanida Mustafovic, Tobias Beisel, Pablo Aguiar, Nikolaos Dikaios, and Matthew W Jacobson, "STIR: software for tomographic image reconstruction release 2," *Physics in Medicine and Biology*, vol. 57, no. 4, pp. 867–883, Feb. 2012.